Catalytic Degradation and Antibacterial Activity of Cinnamon-Mediated Green Synthesized Silver Nanoparticles Loaded on Alginate Beads

Dhoha Alshameri, Fatima Al-Hannan, Fryad Henari and G. Roshan Deen*

Materials for Medicine Research Group, School of Medicine, Royal College of Surgeons in Ireland (RCSI), Medical University of Bahrain, Busaiteen 228, Kingdom of Bahrain

Abstract: Alginate-silver nanocomposites in the form of spherical beads were prepared using a green approach by using the aqueous extract of cinnamon bark. The nanocomposites were fabricated by a three-step process involving gelation by ionotropic crosslinking, adsorption, and in situ chemical reduction in solution. The rich phytochemicals of the cinnamon bark extract played a dual role as reducing and stabilizing agent in the synthesis of silver nanoparticles of average size of 16 nm. The presence of silver nanoparticles in the nanocomposite was studied using UV-Vis absorption spectroscopy, electron microscopy and energy dispersive x-ray spectroscopy. The morphology of the nanocomposite beads was dense and compact with random distribution of silver nanoclusters. The catalytic property of the nanocomposite beads was evaluated for the degradation of Congo-red dye in the presence of sodium borohydride. The degradation followed pseudo-first order kinetics with a rate constant of 0.012 min^{-1} at 23 °C. The activation energy for the degradation process was 27.57 ± 1.5 kJ mol^{-1}. The thermodynamic parameters such as the enthalpy and entropy changes were evaluated using the Eyring equation and were determined to be 0.123 ± 0.05 kJ mol^{-1} and −197.25 ± 2 J mol^{-1} K^{-1}, respectively. The nanocomposite exhibited antibacterial properties against the two strains of bacteria, *Escherichia coli* and *Staphylococcus aureus*.

Keywords: Cinnamon bark, Silver nanoparticles, Green synthesis, Nanocomposite, Congo red degradation, Antibacterial.

1. INTRODUCTION

Depletion of potable water resources due to contamination from various chemical industries pose a global threat. The toxic chemicals discharged from pharmaceutical, electrochemical, textile, and leather industries has adverse effects on human and aquatic life [1,2]. The toxic chemicals include azo dyes, nitrogen-based compounds, aromatic hydrocarbons, and heavy metals. Humans when exposed to these toxic chemicals above the threshold limits, the effects are detrimental and causes damage to the nervous system, developmental effects, discoloration of skin etc. About 10-15% of azo dyes is released by the textile industries alone into the environment.

Several methods are in use to remove toxic chemicals and for the safe discharge of industrial wastewater. A few of these most notable methods are solid-support adsorption, ion-exchange, solvent extraction and photocatalysis [3]. Although adsorption and ion-exchange processes are economical, the degradation of the adsorbed chemical species and reusability of the material are not achieved.

In recent years, advanced oxidation processes such as heterogenous catalysis using metallic and metal oxide nanoparticles such as silver, gold, platinum, palladium, copper, nickel, cobalt, iron, zinc oxide (ZnO), and titanium dioxide (TiO_2), have been recognized as one of the most favorable methods for the degradation of dyes under ambient conditions [4-6]. Polymer supports such as polypropylene, polyamide, cellulose acetate, polysulfone and sodium alginate containing metallic nanoparticles has been widely studied for catalytic degradation of toxic chemicals due to their facile and economic viability [6-8]. Silver nanoparticles are known for their catalytic and antimicrobial properties since very long time, and nanocomposites based on sodium alginate and silver nanoparticles have been exploited as point-of-use disinfection of drinking water and reusable photocatalyst [9,10].

Sodium alginate-based gels have attracted a range of biomedical applications such as drug delivery, implants, wound dressing, 3D bioprinting, organoid morphogenesis, and flexible and wearable electronics devices [11-15]. Sodium alginate is a linear polysaccharide and anionic polymer derived from brown seaweed. It consists of mannuronic (M) and guluronic (G) acids arranged in different combinations such as blocks rich in either M or G units, or blocks of alternating G and M units. In the presence of divalent Ca^{2+} cations, the guluronic acids from nearby chains

*Address corresponding to these authors at the Materials for Medicine Research Group, School of Medicine, Royal College of Surgeons in Ireland (RCSI), Medical University of Bahrain, Busaiteen 228, Kingdom of Bahrain; E-mail: rdeen@rcsi.com

E-ISSN: 1929-5995/24

form ionic crosslinks (ionotropic crosslinking) resulting in alginate hydrogel. The physicochemical properties of the sodium alginate hydrogel are defined by the ratio of M and G units.

Green synthesis or phytosynthesis of nanoparticles and nanocomposites has become a favourable option in recent years due to the environmentally friendly protocol, sustainability, reliability and economic feasibility. Aqueous extracts of medicinal plants and plant products have been preferably used over the past few years in the development of nanocomposites containing metallic nanoparticles. The rich phytochemicals and secondary metabolites present in plant extracts act as excellent chemical reducing and stabilising agent in the formation of nanoparticles from the precursor salts [16]. Cinnamon bark is a spice obtained from the inner bark of several tree species from the genus Cinnamomum, and the active extract contains many active ingredients such as coumarin, cinnamic acid, eugenol, and cinnamaldehyde [17]. These active compounds have various pharmacological properties and some of these are, anti-tumour, anti-diabetic, anti-microbial, and anti-inflammatory.

In this study, we have developed alginate-based silver nanocomposite beads that exhibits satisfactory catalytic and anti-bacterial properties using the aqueous extract of cinnamon bark. The synthesis methodology, catalytic degradation of a model anionic dye (Congo red), and the anti-bacterial potential of this material is described in this work. To the best of our knowledge, this is the first study in the fabrication of alginate-silver nanocomposite beads using the aqueous extract of cinnamon bark.

2. EXPERIMENTAL

2.1. Materials

Cinnamon bark (*Cinnamon verum*) was purchased from a grocery store in Bahrain. Silver nitrate ($AgNO_3$), sodium selenite (Na_2SeO_3), sodium alginate ($NaC_6H_7O_6$, medium molar mass), sodium hydroxide (NaOH), sodium borohydride ($NaBH_4$), Congo red ($C_{32}H_{22}N_6Na_2O_6S_2$) and calcium chloride ($CaCl_2$) were purchased from Sigma and used as received. Deionized water collected from a Millipore system (Elix Technology, Germany) with a conductivity of 18.2 MΩ cm^{-1} was used for all aqueous sample preparations. The antibacterial properties of the synthesized nanoparticles was evaluated against two types of bacteria, *Staphylococcus aureus* (*S. aureus*), and *Escherichia coli* (*E. coli*). The bacteria (*S. aureus* ATCC 29213, and *E. coli* ATCC 25922) were obtained from the American Type Culture Collection (ATCC), USA.

2.2. Preparation of Cinnamon Extract

The cinnamon bark was ground to a fine powder using a coffee grinder and stored in a glass container. About 1.00 g of the cinnamon powder was added to 100 ml of water in a beaker and boiled for 60 min under magnetic stirring. The mixture was air cooled and centrifuged for 10 min at an rpm of 4200 to remove any suspended materials. The clear extract was used fresh in the synthesis of silver nanoparticles.

2.3. Synthesis of Alginate-Silver Nanocomposite Beads

Alginate beads containing silver nanoparticles were prepared by a three-step sequential adsorption and chemical reduction method. The synthesis of alginate-silver nanocomposite beads is described as a representative example as follows.

Stage 1: Sodium alginate (2 wt%) solution was added dropwise into calcium chloride solution (3 wt%) using a plastic syringe (20 ml) with a metal needle (21G) under gentle magnetic stirring. Spherical alginate beads were formed immediately due to ionotropic crosslinking, and the reaction was allowed to continue for 24 h. The beads were washed in water and air dried at room temperature (23 °C) for 1 day.

Stage 2: The air-dried beads obtained stage 1 was suspended in 50 ml of silver nitrate solution (1 mM) under gentle magnetic stirring for 1 day. The beads were isolated and washed repeatedly in water to remove any excess silver nitrate on the beads.

Stage 3: The silver ion adsorbed beads obtained from stage 2 was suspended in 50 ml of aqueous cinnamon extract under gentle stirring for 1 day to reduce the silver ions to silver nanoparticles on the beads. The change in color of the beads from pale yellow to dark yellow and then to light orange indicated the formation of silver nanoparticles. The beads were washed in water and dried in an oven at 50 °C until constant weight was maintained.

2.4. UV-Vis Absorption Spectroscopy

The formation of silver nanoparticles in the beads was confirmed by measuring the absorbance of the

silver nanoparticle solution using a double-beam Shimadzu UV-1800 spectrophotometer. A known weight of the beads was soaked in phosphate buffer solution (5 ml) for 1 day to allow decrosslinking of the beads and release of silver nanoparticles. The solution was filtered using a syringe filter (0.5 μm) and placed in a quartz cuvette (Helma) of 1 cm path length. The absorption spectrum was recorded in the wavelength range 250-1000 nm with a resolution of 1 mm. Water was used as the blank reference for all measurements.

2.5. Scanning Electron Microscopy (SEM)

The size and morphology of the alginate-silver nanocomposite beads were characterized using a scanning electron microscope operating at a voltage of 10 kV (Inovenso, IEM-11). The samples were sputtered with gold for 15 s using an Inovenso SPT-20 coater.

2.6. Transmission Electron Microscopy (TEM)

The silver nanoparticles of the nanocomposite was characterized by TEM in the bright-field mode (model: FEI Morgagni 268, accelerating voltage: 80 kV). The sample was prepared by depositing a drop of the colloidal silver nanoparticles on a copper grid (carbon supported) and air-dried. The image

2.7. Energy-Dispersive X-ray Spectroscopy (EDX)

The silver nanoparticles were characterised for purity by energy-dispersive X-ray (EDX) detector (TESCAN, VEGA 3, 20 kV, Tescan Orsay Holding, Brno, Czech Republic)

2.8. Catalytic Degradation Studies of Congo red (CR)

The catalytic degradation of CR by the alginate-silver nanocomposite beads was followed using a UV-Vis spectrophotometer. A solution of CR (0.07 mM, 2.5 ml) was placed in a quartz cuvette of 1 cm pathlength and the absorbance was recorded. After this, 0.5 ml of freshly prepared $NaBH_4$ (0.1 M) was added to the solution and the absorbance was recorded again. About 5 nanocomposite beads were then added to the solution and the change in absorbance was recorded for a period of 3h. The percentage degradation of CR was calculated using the following equation,

$$\text{Degradation } (\%) = \frac{A_0 - A_t}{A_0} \times 100 \quad (1)$$

where, A_0 and A_t are the absorbance at time zero and absorbance at time *t*, respectively.

2.9. Antibacterial Activity

The antibacterial activity of the synthesized silver nanoparticles against two different types of bacteria such as *S. aureus*, and *E. coli* was carried out using Kirby-Bauer Disk Diffusion Susceptibility Test method. The bacteria strains were spread on a nutrient agar (LB agar) medium using a sterile spreader in all directions. The filter paper discs were loaded with silver nanoparticles (1 mM) (obtained by dissolving the beads in phosphate buffer solution) with aseptic precautions and then the agar plate was incubated at 37 °C for 24 h. The zone of inhibition was observed and measured after 24 h of incubation.

3. RESULTS AND DISCUSSION

3.1. Cinnamon-Mediated Green Synthesis of Alginate Nanocomposites

In this study, alginate-based nanocomposite beads containing silver nanoparticles were prepared by an adsorption and in-situ chemical reduction methods. Neat alginate beads were first prepared by ionotropic crosslinking with divalent cations such as calcium ions (Ca^{2+}). The divalent cations bind to the guluronate blocks of the sodium alginate chains, as the blocks allows a high degree of coordination with the cations. The guluronate blocks of one polymer then forms physical junctions (crosslink points) with the guluronate blocks of adjacent polymer chains. This type of crosslinking and formation of a gel is termed the egg-box model of crosslinking [18]. The nanoparticles were then formed by in-situ chemical reduction using the aqueous extract of cinnamon. Cinnamon bark contains a wide variety of phytochemicals such as cinnamaldehyde, cinnamic acid, cinnamate and various essential oils [17]. These phytochemicals act as efficient chemical reducing agents and conveniently reduce the silver ions to the corresponding nanoparticles. The synthesis methodology is illustrated in Figure (**1a**) and the digital images of the beads are shown in Figure (**1b,c**).

The surface morphology of the nanocomposite beads was studied using scanning electron microscopy and the results are shown in Figure (**2**). The dry beads were close to spherical shape with an average size of 1.0 μm as shown by the SEM micrograph in Figure (**2a**). The surface of the nanocomposite beads were compact with dense particulate clusters as shown under high magnification (1.0 k) (Figure **2b**).

To confirm the presence of silver nanoparticles and their size, the alginate beads were soaked in

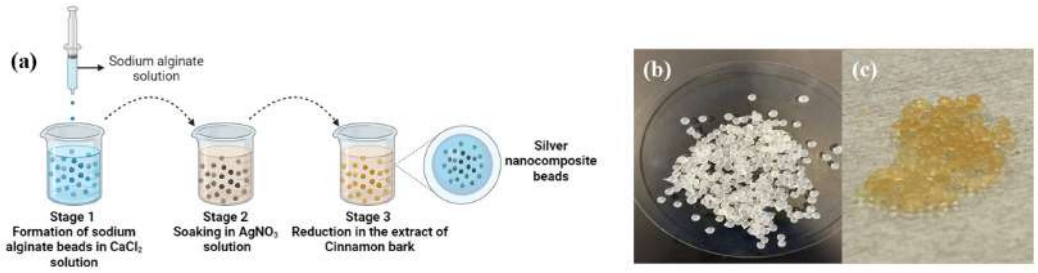

Figure 1: (**a**) Illustration of synthesis methodology of the nanocomposite beads; (**b**) digital image of alginate beads; (**c**) silver nanocomposites.

phosphate buffer solution and dissociated to release the silver nanoparticles from the composite. The dissociation causes chelation of Ca^{2+} by PO_4^{3-} and HPO_4^{2-} ligands, any releasing the alginate and silver nanoparticles in solution. The resulting viscous solution was analyzed by UV-Vis absorption spectroscopy and the result is shown in Figure (**3**). A strong SPR peak around 420 nm confirmed the presence of silver nanoparticles in the alginate-nanocomposite beads.

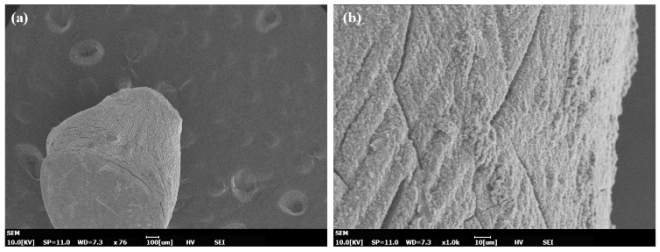

Figure 2: (**a**) Scanning electron micrograph of alginate-silver nanocomposite beads; (**b**) under magnification of 1.0 k showing the compact surface.

As observed by TEM, the silver nanoparticles were spherical with an average size of 16 nm, and purity was about 80% as confirmed by EDX. The results are shown in Figure (**4a,b**). These results indicate that very small silver nanoparticles can effectively be green synthesized by cinnamon extract and supported on solid polymers.

3.2. Catalytic Degradation of Congo red (CR)

Congo red dye is an anionic dye that is used extensively in various industries such plastic, leather, printing, and paper. It is a benzidine-based anionic dye with two azo groups in its chemical structure, and structure is shown in Figure (**5a**). This dye is toxic both to humans and aquatic life, and hence needs to be degraded before being discharged into water bodies and land [1,2,19]. The degradation of CR was studied using the silver nanocomposites as catalyst to evaluate their catalytic performance. The change in absorbance of CR solution (λ = 489 nm) containing sodium borohydride and silver nanocomposite beads (5 beads) is shown in Figure (**5b**).

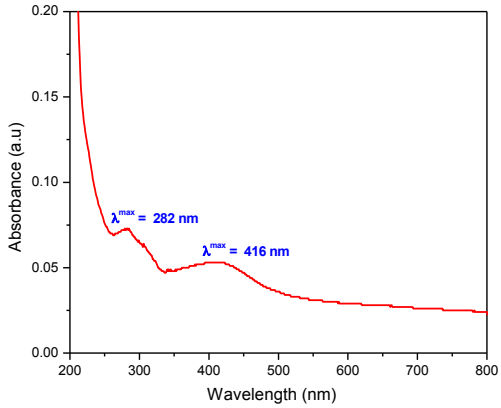

Figure 3: UV-Vis absorption spectra of silver nanoparticles in water.

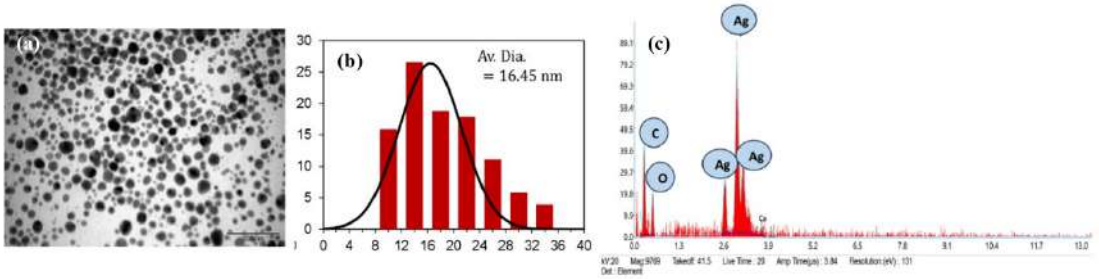

Figure 4: (**a**) Transmission electron micrograph of silver nanoparticles, (**b**) size distribution, (**c**) EDX of silver nanoparticles.

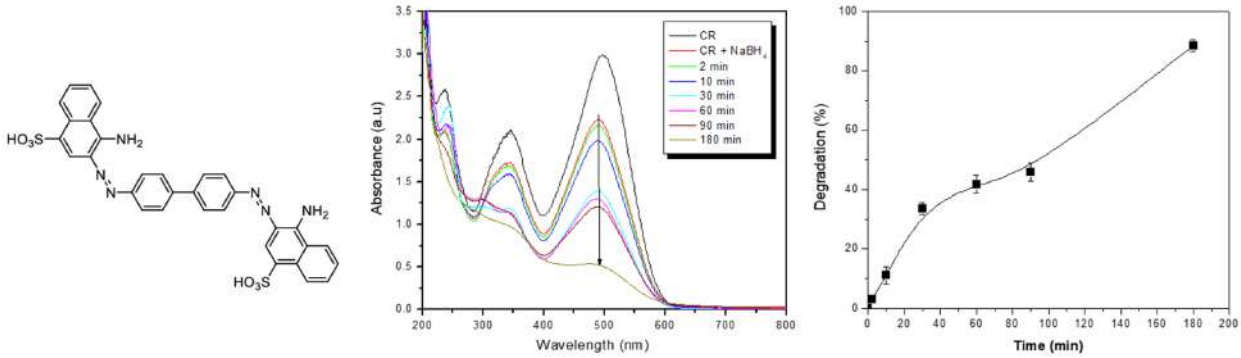

Figure 5: (**a**) Chemical structure of Congo red; (**b**) Degradation of CR by alginate-silver nanocomposite beads in the presence of $NaBH_4$; (**c**) Percentage degradation of CR as function of time.

A progressive decrease in absorbance at 489 nm is observed which indicates the degradation of CR over time by the silver nanoparticles embedded in the alginate beads. The initial absorbance of 2.23 decreased significantly to 0.53 in about 180 min. The percentage degradation of CR was calculated using the following equation,

$$\text{Degradation } (\%) = \frac{A_0 - A_t}{A_0} \times 100 \quad (1)$$

where A_0 and A_t are the initial absorbance and absorbance at time t, respectively.

The degradation kinetics is shown in Figure (**5c**) and a degradation of 88% is observed in about 180 min of the reaction. The degradation could be enhanced by improving the porosity of the beads. This would provide faster diffusion of CR into the beads for reaction with the active proton species. The electrons from the reducing agent (BH_4^-) reacts with the azo group (–N=N–) of CR reducing it to a single bond (–N–N–). As the electron conjugation is lost, decolorization of the dye is observed [20]. Interestingly, in the absence of the nanocomposite beads the degradation was significantly slow and it took about 3 days to observe a change in absorbance of the sample. This confirms the catalytic role of silver nanoparticles in the degradation of CR.

The rate constant (k) of the degradation process was determined using the following linear equation as,

$$\ln \frac{C_t}{C_0} = ln \frac{A_t}{A_0} = -kt \quad (2)$$

where C_t and C_0 are the concentration of CR, and A_t and A_0 are the absorbances at time t, and t = 0, respectively, k (min^{-1}) is the rate constant of the reaction.

From a plot of $\ln(A_t/A_0)$ versus reaction time (t) in min the rate constant was determined from the negative slope as 0.012 min^{-1} (Figure **6**). The degradation reaction followed a pseudo-first order reaction kinetics with respect to the alginate-silver nanocomposite beads as the concentration of $NaBH_4$ (10 mM) was much higher than that of CR (1 mM). The reaction kinetics and the rate constant obtained agreed with reported values for catalytic reduction of CR by green synthesized silver, gold, copper and cobalt nanoparticles, and polymer nanocomposites [21-23].

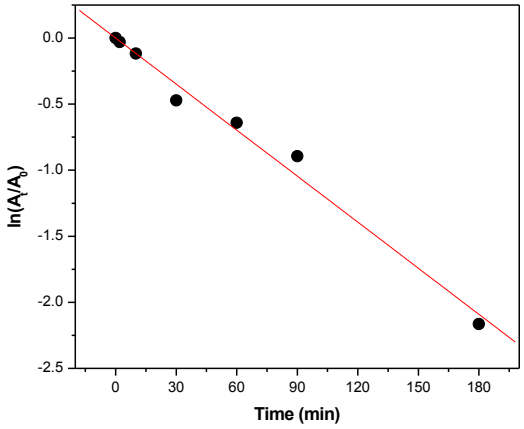

Figure 6: Pseudo-first order reaction kinetics of CR degradation in the presence of $NaBH_4$ at 23 °C.

3.3. Thermodynamic Parameters for CR Degradation by the Nanocomposite Beads

The activation energy (E_a) for the degradation of CR by the nanocomposite beads was determined using Arrhenius equation [24] as,

$$\ln(k) = \left(\frac{E_a}{R}\right)\frac{1}{T} + \ln(A) \quad (3)$$

where A = frequency factor or Arrhenius constant, R = 8.314 J K^{-1} mol^{-1}, T = absolute temperature in Kelvin, and k = rate constant.

From a linear plot of ln(*k*) versus 1/*T*, the E_a and *A* were determined from the slope and intercept as 27.57 kJ mol^{-1} and 6.84 min^{-1}, respectively (Figure **7a**).

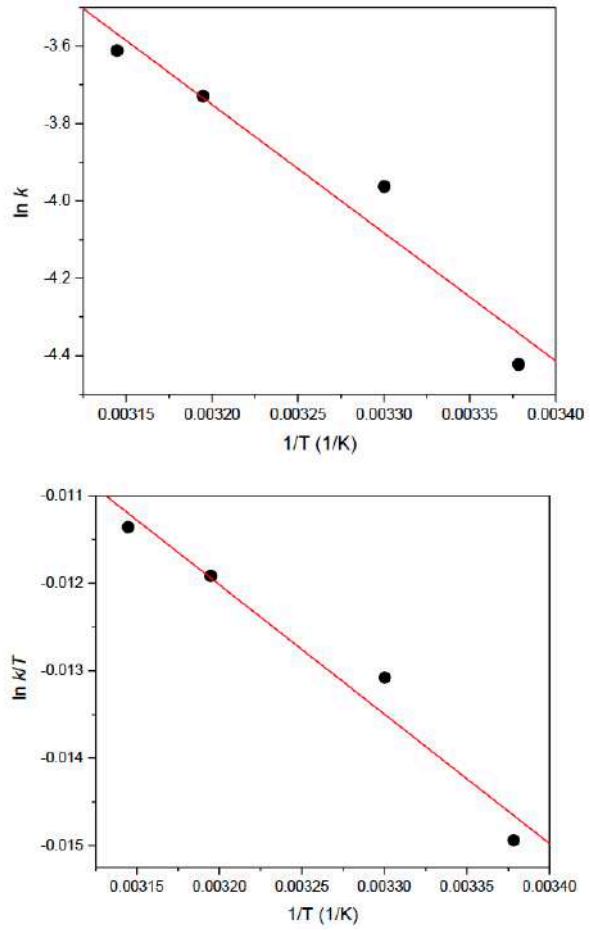

Figure 7: (**a**) Arrhenius plot for the determination of activation energy; (**b**) Eyring plot for the determination of enthalpy and entropy.

The thermodynamic parameters such as enthalpy change, (ΔH), and entropy change (ΔS) for the degradation reaction were determined using Eyring equation as [25],

$$\ln\frac{k}{T} = ln\frac{k_B}{h} + \frac{\Delta S}{R} - \frac{\Delta H}{R}\left(\frac{1}{T}\right) \quad (4)$$

where k_B is the Boltzmann constant (1.381 × 10^{-23} JK^{-1}), *h* is the Planck's constant (6.626 × 10^{-34} J.s), *R* is the ideal gas constant, and *T* is the absolute temperature in Kelvin.

From a linear plot of ln(*k*/*T*) versus 1/*T* (Figure **7b**), the enthalpy (ΔH), and entropy(ΔS) change for the degradation of CR were determined to be 0.123 kJ mol^{-1} and –197.25 J mol^{-1} K^{-1}, respectively. The kinetic and thermodynamic parameters for the catalytic reduction of CR by the alginate-silver nanocomposite beads are shown in Table **1**. The negative slope indicates the degradation process using the nanocomposites is endothermic. The negative entropy values indicate that the randomness on the interface between the nanocomposite bead and CR decrease during the dye degradation [26]. The values are comparable to CR degradation by green synthesized silver nanoparticles and nanocomposites using various plants and plant products such as papaya leaf, mustard oil, *Amaranthus gangeticus* leaf, and *Anacardium occidentale* leaf [1,27-29].

The conversion efficiency of the alginate-silver nanocomposite beads was evaluated for 5 successive cycles and the results are shown in Figure (**8**). After each cycle of CR degradation, the beads were removed from the solution and washed repeatedly with water and then placed into a fresh solution containing CR and $NaBH_4$.

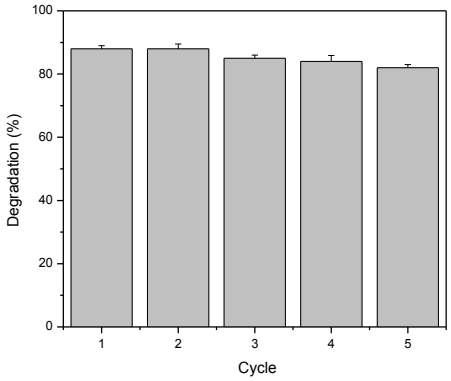

Figure 8: Degradation efficiency of the nanocomposite beads for 5 cycles.

The conversion efficiency of the nanocomposite beads was within the range of 88-82% up to 5

Table 1: Kinetic and Thermodynamic Parameters for Catalytic Degradation of CR by the Alginate-Silver Nanocomposite Beads in the Presence of $NaBH_4$

Temperature (K)	*k* (min^{-1})	E_a (kJ mol^{-1})	ΔH (kJ mol^{-1})	ΔS (J mol^{-1} K^{-1})
296	0.012	27.57 ± 1.5	0.123 ± 0.05	– 197.25 ± 2.0
303	0.019			
313	0.024			
318	0.027			

successive cycles, which indicates good catalytic efficiency and material sustainability on repeated usage. During this study, leaching of silver nanoparticles from the beads or any disintegration of the beads were not observed.

3.4. Antibacterial Properties

The silver nanoparticles exhibited good antibacterial properties against *E. coli*, and *S. aureus*. The bacterial agar plates with the zone of inhibition is shown in Figure (**9**). The sodium alginate as control showed a weak antibacterial effect against the two types of bacteria. The alginate-silver nanocomposite beads exhibited a larger zone of inhibition relative to the neat alginate beads which indicates the synergistic antibacterial effect of the nanocomposites. Similar synergistic effects have been observed for many green synthesized silver nanocomposites [30].

The mechanism of interaction of silver nanoparticles with the bacteria is mainly ionic. The silver nanoparticles and silver ions (released from the nanoparticles) can accumulate in the pits of the cell wall and leads to denaturation of the cell membrane [31]. In addition, the silver nanoparticles could penetrate the cell membrane leading to denaturation and rupture of organelles resulting in lysis. Further, the silver nanoparticles can disrupt bacterial signal transduction leading to cell apoptosis and termination of the bacterial cell multiplication.

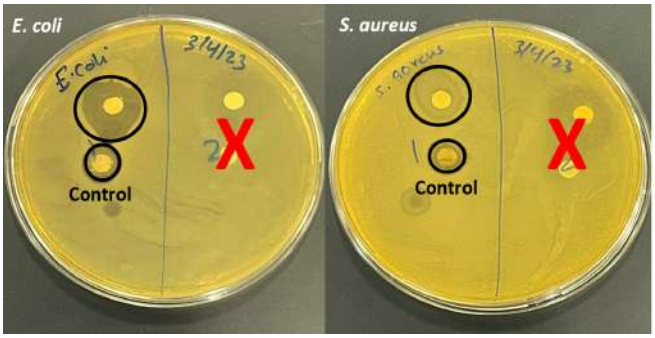

Figure 9: The antibacterial activity of silver nanoparticles on *E. coli* and *S. aureus* showing the zone of inhibition.

4. CONCLUSIONS

Alginate-silver nanocomposites in the form of close to spherical beads was successfully synthesized using the extract of cinnamon bark as the chemical reducing agent. The nanocomposite beads were effective in the catalytic degradation of Congo red dye and 88% degradation was achieved in about 180 min. The beads showed good reusability with no appreciable decrease in the degradation capacity even up to 5 successive cycles. The degradation followed a pseudo-first order reaction kinetics. The nanocomposite exhibited antibacterial effects against two clinically important pathogens with similar susceptibility. Overall, this study has laid the foundation for a new effective strategy as an alternative to high-cost commercial catalysis for the detoxification of organic pollutants. The new material developed through the eco-friendly green approach in addition to the catalytic properties has the potential to treat clinical wastewater in the future. The potential limitation of longer degradation time could be shortened by making the beads more porous to facilitate faster diffusion of pollutants inside the beads.

CONFLICT OF INTEREST

The authors declare that they have no conflict of interest.

LIST OF ABBREVIATION

CR = Congo red

EDX = Energy Dispersive X-ray Spectroscopy

SEM = Scanning Electron Microscopy

TEM = Transmission Electron Microscopy

SPR = Surface Plasmon Resonance

UV-Vis = Ultraviolet-Visible

REFERENCES

[1] Gaur J, Vikrant K, Kim K-H, *et al*. Photocatalytic degradation of Congo red dye using zinc oxide nanoparticles prepared using Carica papaya leaf extract. Materials Today Sustainability 2023; 22: 100339. https://doi.org/10.1016/j.mtsust.2023.100339

[2] Dhruv Patel D, Bhatt S. Environmental pollution, toxicity profile, and physico-chemical and biotechnological approaches for treatment of textile wastewater. Biotechnology and Genetic Engineering Review 2022; 38: 33-86. https://doi.org/10.1080/02648725.2022.2048434

[3] Kumar M, Venugopal AKP, Pakshirajan K. Novel biologically synthesized metal nano powder from wastewater for dye removal application. Environmental Science Pollution Control Series 2022; 29: 38478-38492. https://doi.org/10.1007/s11356-022-18723-z

[4] Choudhary MK, Kataria J, Sharma S. Evaluation of the kinetic and catalytic properties of biogenically synthesized silver nanoparticles. Journal of Cleaner Production 2018; 198: 882-890. https://doi.org/10.1016/j.jclepro.2018.09.015

[5] Gupta VK, Yola ML, Eren T, Kartal F, *et al*. Catalytic activity of Fe@Ag nanoparticle involved calcium alginate beads for the reduction of nitrophenols. Journal of Molecular Liquids 2014; 190 (1): 133-138. https://doi.org/10.1016/j.molliq.2013.10.022

[6] Augustine R, Kalarikkal N, Thomas S. A facile and rapid method for the black pepper leaf mediated green synthesis of silver nanoparticles and the antimicrobial study. Applied Nanoscience 2014; 4: 809-818. https://doi.org/10.1007/s13204-013-0260-7

[7] Kastner C, Thunemann F. Catalytic reduction of 4-nitrophenol using silver nanoparticles with adjustable activity. Langmuir 2016; 32: 7383-7391. https://doi.org/10.1021/acs.langmuir.6b01477

[8] Lin S, Huang R, Cheng W, *et al*. Silver nanoparticle-alginate composite beads for point-of-use drinking water disinfection. Water Research 2013; 47: 3959-3965. https://doi.org/10.1016/j.watres.2012.09.005

[9] Mthombeni NH, Mpenyana-Monytasi I, Onyango MS, *et al*. Breakthrough analysis for water disinfection using silver nanoparticles coated resin beads in fixed-bed column. Journal of Hazardous Materials 2012; 217-218: 133-140. https://doi.org/10.1016/j.jhazmat.2012.03.004

[10] Albalwi H, El Fadl FIA, Ibrahim MM, *et al*. Catalytic activity of silver nanocomposite alginate beads for degradation of basic dye: Kinetic and isothermal study, Applied Organometallic Chemistry 2021; e6490: 1-11. https://doi.org/10.1002/aoc.6490

[11] Martinez-Gómez F, Guerrero J, Matsuhiro B, *et al*. *In vitro* release of metformin hydrochloride from sodium alginate/polyvinyl alcohol hydrogels. Carbohydrate Polymers 2017; 155: 182-191. https://doi.org/10.1016/j.carbpol.2016.08.079

[12] Fagieh TM, Bakhsh EM, Khan SB, *et al*. Alginate/banana waste beads supported metal nanoparticles for efficient water remediation. Polymers 2021; 13: 4054-4071. https://doi.org/10.3390/polym13234054

[13] Khan SB, Ahmad S, Karnal T, *et al*. Metal nanoparticles decorated sodium alginate-carbon nitride composite beads as effective catalyst for the reduction of organic pollutants. International Journal of Biological Macromolecules 2020; 164: 1087-1098. https://doi.org/10.1016/j.ijbiomac.2020.07.091

[14] Alomar A, Qassim T, AlNajjar Y, *et al*. Green nanotechnology and phytosynthesis of metallic nanoparticles: The green approach, mechanism, biomedical applications and challenges. World Scientific Annual Review of Functional Materials 2024; 1: 2430001-2430023. https://doi.org/10.1142/S2810922824300010

[15] Deen GR, AlHannan F, Henari F, *et al*. Effects of different parts of the okra plant (*Abelmoschus esculentus*) on the phytosynthesis of silver nanoparticles: Evaluation of synthesis conditions, nonlinear optical and antibacterial properties. Nanomaterials 2022; 12: 4174-4185. https://doi.org/10.3390/nano12234174

[16] Gunti L, Dass RS, Kalagatur NK. Phytofabrication of selenium nanoparticles from *Emblica officinalis* fruit extract and exploring its biopotential applications: Antioxidant, antimicrobial, and biocompatibility. Frontiers of Microbiology 2019; 10: 931-948. https://doi.org/10.3389/fmicb.2019.00931

[17] Premkumar J, Sudhakar T, Dhakal A. Synthesis of silver nanoparticles from cinnamon against bacterial pathogens. Biocatalysis and Agricultural Biotechnology 2018; 15: 311-316. https://doi.org/10.1016/j.bcab.2018.06.005

[18] Cao PL, Lu W, Mata A, *et al*. Egg-box model-based gelation of alginate and pectin: A review. Carbohydrate Polymers 2020; 242: 116389-116399. https://doi.org/10.1016/j.carbpol.2020.116389

[19] Siddiqui SL, Allehyani ES, Al-Harbi SA, *et al*. Investigation of Congo red toxicity towards different living organisms: A Review. Processes 2023; 11: 807-820. https://doi.org/10.3390/pr11030807

[20] Michel CR, Martinez-Preciado AH. Adsorption and photocatalytic degradation of Congo red and malachite green by nanostructures Y_2O_3 synthesized by the coprecipitation method. Open Ceramics 2023; 13: 100336-100343. https://doi.org/10.1016/j.oceram.2023.100336

[21] Uma Maheswari G, Lakshmanan A, Nagarajan NS, Green synthesis, characterization and catalytic degradation studies of gold nanoparticles against Congo red and methyl orange, Journal of Photochemistry and Photobiology, B: Biology 2018; 178: 33-39. https://doi.org/10.1016/j.jphotobiol.2017.10.017

[22] Nandhini NT, Rajeshkumar S, Mythili S, The possible mechanism of eco-friendly synthesized nanoparticles on hazardous dyes degradation. Biocatalysis and Agricultural Biotechnology 2019; 19: 101138-101147. https://doi.org/10.1016/j.bcab.2019.101138

[23] Liu K, Yang Y, Sun F, *et al*. Rapid degradation of Congo red wastewater by *Rhodopseudomonas palustris* intimately coupled carbon nanotube-silver modified titanium dioxide photocatalytic composite with sodium alginate. Chemosphere 2022; 299: 134417-134422. https://doi.org/10.1016/j.chemosphere.2022.134417

[24] Raymond C, Physical Chemistry for the Biosciences, University Science Books, Sausalito (CA) 2005; pp. 311-347.

[25] Anjum F, Asiri AM, Khan MA, *et al*. Photo-degradation, thermodynamic and kinetic study of carcinogenic dyes via zinc oxide/graphene oxide nanocomposites. Journal of Materials Research and Technology 2021; 15: 3171-3191. https://doi.org/10.1016/j.jmrt.2021.09.086

[26] Albukhari SM, Ismail M, Akhtar K, *et al*. Catalytic reduction of nitrophenols and dyes using silver nanoparticles @ cellulose polymer paper for the resolution of wastewater treatment challenges. Colloids and Surfaces A 2019; A577: 548-561. https://doi.org/10.1016/j.colsurfa.2019.05.058

[27] Lekshmi GS, Ramasamy T, Bazaka O, *et al*. Antioxidant, anti-bacterial and Congo red dye degradation activity of Ag_xO decorated mustard oil-derived rGO nanocomposites, Molecules 2022; 27: 5950-5960. https://doi.org/10.3390/molecules27185950

[28] Marimuthu S, Antonisamy AJ, Malayandi S, *et al*. Silver nanoparticles in dye effluent treatment: A review on synthesis, treatment methods, mechanisms, photocatalytic degradation, toxic effects and mitigation of toxicity. Journal of Photochemistry and Photobiology B: Biology 2020; 205: 111823-111838. https://doi.org/10.1016/j.jphotobiol.2020.111823

[29] Edison TNJI, Atchudan R, Kamla C, *et al*. Reductive degradation of carcinogenic azo dyes using Anacardium occidentale testa derived silver nanoparticles. Journal of Photochemistry and Photobiology B: Biology 2016; 162: 604-610. https://doi.org/10.1016/j.jphotobiol.2016.07.040

[30] Farazin A, Mohammadimehr M, Ghasemi AM, *et al*. Design, preparation and characterization of CS/PVA/SA hydrogels modified with mesoporous Ag_2O/SiO_2 and curcumin nanoparticles for green, biocompatible, and antibacterial biopolymer film. RSC Advances 2021; 11: 32775-32791. https://doi.org/10.1039/D1RA05153A

[31] Cittrarasu V, Kaliannan D, Dharman K, *et al*. Green synthesis of selenium nanoparticles mediated from *Ceropegia bulbosa* Roxb extract and its cytotoxicity, antimicrobial, mosquitocidal and photocatalytic activities. Scientific Reports 2021; 11: 1032-1046. https://doi.org/10.1038/s41598-020-80327-9

Received on 20-10-2024 Accepted on 14-11-2024 Published on 13-12-2024

https://doi.org/10.6000/1929-5995.2024.13.26